EBioMedicine 60 (2020) 102992

Contents lists available at ScienceDirect

EBioMedicine

journal homepage: www.elsevier.com/locate/ebiom

Research paper

Endothelial damage and a thin intercellular fibrin network promote haemorrhage in acute promyelocytic leukaemia

Chunxu Wang[a,b], Muxin Yu[a], Peng Zhou[b,c], Baorong Li[a], Yingmiao Liu[a], Lixiu Wang[d], Xiaojing Chen[a], Jingwen Du[a], Yufeng Wang[a], Jinming Zhang[a], Haijiao Jing[a], Yiming Feng[a], Yue Zhang[a], Yueyue Li[a], Zengxiang Dong[d], Shaohong Fang[b], Valerie A Novakovic[e], Jin Zhou[a], Jialan Shi[a,e,f,*]

[a] Department of Hematology, The First Hospital, Harbin Medical University, 23 Youzheng Street, Nangang District, Harbin 150001, China
[b] The Key Laboratory of Myocardial Ischemia, Ministry of Education, Heilongjiang Province, Harbin, China
[c] Department of Neurosurgery, The Second Hospital, Harbin Medical University, Harbin, China
[d] Departments of Cardiology, The First Hospital, Harbin Medical University, Harbin, China
[e] Department of Research, VA Boston Healthcare System, Harvard Medical School, Boston, MA, USA
[f] Department of Medicine, Brigham and Women's Hospital, Harvard Medical School, 1400 VFW Parkway, West Roxbury, Boston, MA 02132, USA

ARTICLE INFO

Article History:
Received 26 May 2020
Revised 16 August 2020
Accepted 24 August 2020
Available online xxx

Keywords:
Acute promyelocytic leukaemia
Endothelial cells
Permeability
Fibrin
Haemorrhage

ABSTRACT

Background: The role of vascular endothelium in acute promyelocytic leukaemia (APL) remains unknown. We aimed to investigate the mechanisms by which APL cells interact with endothelial cells (ECs) and to further explore how the endothelium affects bleeding as well as therapeutic interventions.
Method: APL cells and an original APL cell line, NB4 cells, were used for experiments. The effects of leukaemic cells on ECs were analyzed in vitro and in vivo. Moreover, the endothelial barrier function and procoagulant activity were detected. An APL mouse model was established for in vivo studies.
Findings: APL cells interacted with ECs via ICAM-1 and VCAM-1 receptors to disrupt endothelial integrity. This binding activated MLCK signaling, resulting in the trans-endothelial passage of protein and red blood cells (RBCs). Combined treatment with asiatic acid or anti-adhesion receptor antibody inhibited the response of ECs to APL cells, thereby preventing APL-associated haemorrhage in vitro and in vivo. Activated ECs exhibited a procoagulant phenotype after phosphatidylserine exposure. Plasma from APL patients formed a thin fibrin network between procoagulant ECs, and this intercellular fibrin decreased the passage of albumin and RBCs. Ex vivo addition of fibrinogen further enhanced this barrier function in a dose-dependent manner.
Interpretation: Endothelial damage induced by leukaemic cell adherence promotes haemorrhaging in APL. Stabilization of ECs, decreasing adhesion receptor expression, and increasing fibrinogen transfusion levels may be a new therapeutic avenue to alleviate this fatal bleeding complication.
Funding: National Science Foundation of China (81670128, 81873433).

1. Introduction

Acute promyelocytic leukaemia (APL) is a disease characterized by catastrophic bleeding. Treatment with all-*trans* retinoic acid (ATRA) or arsenic trioxide (ATO) leads to complete remission in up to 90% of patients [1–3]. However, bleeding events remain a leading cause of early death (25–29% incidence rate) in APL and account for 40–65% of the mortality of this disease [4,5]. Thus, it is essential to study the mechanisms of pathological bleeding in APL.

APL-induced haemorrhage results from the coagulopathy-inducing properties of leukaemic cells, including the expression of tissue factor (TF), fibrinolytic, and proteolytic mediators [5,6]. However, compared to coagulation parameters, the number of APL blasts is a better predictor of bleeding events, suggesting that other unknown pathological outcomes are relevant to haemorrhage caused by leukaemic cells [6,7]. Endothelial monolayers that line the vasculature separate blood from tissues. This barrier, acting as the blood-tissue interface, regulates the exchange of proteins and cells. The breakdown of this barrier plays a crucial role in spontaneous bleeding [8-10]. However, little has been reported about the role of the endothelial barrier in APL haemorrhage. Under various conditions, endothelial cells (ECs) are directly exposed to immune cells, including

* Corresponding author at:Department of Hematology, The First Hospital, Harbin Medical University, 23 Youzheng Street, Nangang District, Harbin 150001, China.
E-mail address: jialan_shi@hms.harvard.edu (J. Shi).

https://doi.org/10.1016/j.ebiom.2020.102992

Research in context

Evidence before this study

So far, early hemorrhagic death remains a major obstacle to complete remission in acute promyelocytic leukemia (APL). The number of leukemia cells in the blood is a better predictor of bleeding events than other hematological parameters. Vascular endothelial homeostasis is associated with spontaneous bleeding. In APL, how APL cells interact with vascular endothelial cells and whether this interaction affects bleeding complications remains unknown.

Added value of this study

In this study, APL cells induced endothelial cell (EC) contraction and pore formation, resulting in endothelial hyperpermeability in vitro and hemorrhage in vivo. Asiatic acid, extracted from a Chinese herb, anti-ICAM1, and anti-VCAM1 antibodies blocked leukemic cells from activating ECs and alleviated the bleeding in APL mice models. ECs stimulated by APL cells converted to procoagulant phenotype through phosphatidylserine exposure. Intercellular fibrin networks generated along the edge of the retracted ECs sealed the barrier injury and reduced the permeability of endothelial monolayers to RBCs. In addition, all-*trans* retinoic acid rescued the morphological alterations of ECs that occurred in the process of exposure to NB4 cells.

Implications of all the available evidence

Endothelial integrity plays a key role in preventing bleeding complications in APL. Blocking leukemic cell adhesion to the vascular wall and regulating endothelium homeostasis may provide novel potential therapeutic targets for intervention in hemorrhage of APL. In addition, reassessment of the target level of transfused Fbg according to different risk stratifications may also be necessary.

neutrophils and lymphocytes, or tumor cells such as leukaemic cells. These cells interact with the endothelium and increase the permeability of the microvasculature, resulting in haemorrhage via disruption of junction proteins [11-13]. Whether APL cells induce similar effects in the peripheral vasculature is unknown. The exact mechanisms underlying possible morphological and functional changes in ECs also remain to be defined.

Asiatic acid is a pentacyclic triterpenoid extracted from the Chinese herb *Centella asiatica.* Asiatic acid has a wide range of beneficial anti-inflammation and anti-cancer effects [14,15]. Recently, asiatic acid has been reported to prevent the inflammatory factor damage in the endothelial barrier [16]. Nevertheless, the role of asiatic acid in APL is unclear. Platelets play a key role in safeguarding vascular integrity [17,18]. They adhere to the endothelium and fill gaps, thereby preventing haemorrhage in inflammation and cancer [17]. However, fibrinogen (Fbg) transfusion exhibited effects similar to platelets in alleviating haemorrhage [19,20]. Moreover, our previous studies showed that fibrin strands distributed along the margin of procoagulant ECs formed a cellular fibrin network [21,22]. Therefore, we hypothesized that fibrin networks between ECs play a role in endothelial integrity. Furthermore, the associated regulatory mechanisms for this fibrin formation are worth studying.

Here, we showed that APL cells disrupted endothelial integrity by inducing openings between ECs. Asiatic acid, as well as anti-adhesion receptor antibodies, inhibited the resulting endothelial hyper-permeability and haemorrhage in vitro and in vivo. Moreover, ECs under APL cell stimulation were transformed to a procoagulant phenotype via phosphatidylserine (PS) exposure. Fibrin networks between procoagulant ECs showed beneficial effects on endothelial integrity. Because ATRA and ATO are widely used in APL therapy, their role in the endothelial barrier was also examined. Our study may help provide novel potential therapeutic targets for intervention in bleeding complications of APL.

2. Materials and methods

2.1. Reagents

Human umbilical vein endothelial cells (HUVECs) and poly-L-lysine-coated flasks were obtained from ScienCell (San Diego, CA). The human APL NB4 cell line was a gift from Dr. James O'Kelly (Los Angeles, CA). Foetal bovine serum, RPMI 1640 medium, and EC medium were obtained from Gibco (Grand Island, NY). Polyclonal anti-human TF (4502), anti-ICAM-1, anti-VCAM-1, anti-ZO-1, anti-VE-cadherin, and FITC-conjugated anti-human TF (4508CJ) antibodies were all obtained from Abcam (Stamford, CT). Anti-β-actin antibodies were obtained from Sigma-Aldrich (St. Louis, Missouri). Asiatic acid was purchased from FeiYu Biotech Ltd Co (Nantong, China). The anti-phosphorylated VE-cadherin antibody was obtained from Invitrogen (Carlsbad, CA). ATRA and ATO were obtained from Sigma-Aldrich (St. Louis, MO). Fluorescein-labelled Fbg, FVa, FXa, and lactadherin conjugated with Alexa Fluor 488 or Alexa Fluor 647 were all prepared in our laboratory. TRITC-phalloidin was obtained from Shanghai Yu Sheng (Shanghai, China). ESM1-endocan, human soluble VCAM-1 (sVCAM-1), human soluble thrombomodulin (sTM) and human soluble ICAM-1 (sICAM-1) ELISA kits were from Aviscera Bioscience Inc. (Santa Clara, CA). PVDF membranes and anti-mouse antibodies were obtained from Amersham (Little Chalfont, UK).

2.2. Patients

Thirty-two newly-diagnosed APL patients, admitted to the First and Second Affiliated Hospital of Harbin Medical University between August 2017 and August 2019, consented to participate in this study. The diagnoses were based on immunology and cytochemistry results, clinical data, morphology, molecular pathology, and cytogenetics findings, which confirmed the presence of at(15;17) (PML-RARA) fusion gene in all study cases [23]. Haematuria, spontaneous ecchymosis, mucosal bleeding, melena, haematemesis, petechiae, and menorrhagia manifest as haemorrhage. This study was approved by the Ethics Committee of Harbin Medical University and complied with the Declaration of Helsinki. Informed consent from all participants was obtained. Patient characteristics and blood parameters on the day of bone marrow (BM) aspiration are presented in Table 1.

2.3. Cell culture

We isolated fresh APL blasts from BM specimens by Ficoll-Hypaque centrifugation. Complete RPMI 1640 medium was used to culture isolated cells (5×10^5/mL). The culture medium was supplemented with 20% FBS, 1% penicillin-streptomycin solution, and 2 mM L-glutamine, and cells were incubated in a 5% CO_2 humidified atmosphere at 37 °C. Cells from an APL cell line (NB4 cells) were maintained in the same conditions. HUVECs were maintained in EC medium including DMEM medium with high glucose, 10% FBS, 1% endothelial cell growth factor, and 0.5% antibiotics. We propagated these cells in poly-L-lysine-coated cell culture flasks at 37 °C and 5% CO_2 in a humid environment. Cells between passages two and four were used to perform the following experiments.

2.4. Coincubation assay

HUVECs (5×10^5/12 wells) were plated on coverslips in 24-well plates and grew into a monolayer within 3 days. Before the start of the

Table 1
Characteristics of APL patients and controls.

	Control (n = 30)	APL (n = 32)
Age, y	41 ± 3	49.5 ± 15.39
Gender, male/female	16/14	21/11
BMI, kg/m^2	26.4 ± 0.21	24.4 ± 0.2
Diagnosis		
M3/bcr1, n%	–	10 (31.25)
M3/bcr2, n%	–	11 (34.38)
M3/bcr3, n%	–	11 (34.38)
WBC, × 109	6.3 ± 0.11	22.3 ± 8.1*
Hb, g/L	132.5 ± 0.85	89.8 ± 5.6 *
PLTs, × 109	230 ± 3.7	42.2 ± 8.1 *
Blasts, BM%	–	42.4 ± 4.86
PT, s	12.73 ± 0.1	13.89 ± 0.4 *
APTT, s	28.2 ± 0.5	29.8 ± 1
Fibrinogen, g/L	2.9 ± 0.1	1.9 ± 0.2 *
D-dimer, mg/mL	0.25 ± 0.01	5.7 ± 0.9 *

The major clinical and laboratory characteristics of 30 healthy controls and 32 newly diagnosed APL patients are shown. Data are presented as numbers (percentages) or the median ± SD or median values (25th and 75th percentiles). BMI, body mass index (r.v. 18.5–25 kg/m^2); Bcr, breakpoint cluster region (bcr1 = intron 6, bcr2= exon 6, bcr3 = intron 3); WBC, white blood cell; PLT, platelet; Hb, haemoglobin; PT, prothrombin time (r.v. 10–15 s); Blasts, promyelocytes + blasts; BM, bone marrow; APTT, activated partial thromboplastin time (r.v. 20–40 s).

* $P < 0.05$ vs. healthy controls.

coculture experiment, fresh APL cells and NB4 cells were cultured in complete RPMI 1640 medium for 24 h. The supernatant was then collected by centrifugation (800r, 4 min). Confluent endothelial monolayers with/out pretreatment with asiatic acid were incubated with the supernatant, complete RPIM1640 medium, fresh APL/NB4 cells for another 24 h, respectively. Then, we removed the mixture medium, and phosphate-buffered saline (PBS) was used to wash adherent APL/NB4 cells on the coverslips, which were used for subsequent experiments. Flow cytometry was then used to detect PS exposure.

2.5. Endothelium permeability assay

Endothelial cells were propagated on transwell polyester membranes with 3 μm pore size and 6.5 mm diameter at an average density of 2 × 10^5 cells/well (Costar, Corning, NY). Cells were grown to confluence until the 3rd day and then treated with NB4/APL-CM. Growth medium containing 4% BSA (Gibco) was mixed with Evens blue (Sigma, St Louis, MO). At different time points, the permeability was measured by adding fresh medium-free BSA to the lower chamber and Evens blue BSA mixture to the upper chamber in each well. After 10 min, the optical density of Evens blue BSA in the lower chamber was measured using a fluorescence microplate reader at 650 nm.

2.6. Red blood cell (RBC) leakage assay

Blood was drawn from healthy volunteers and collected in 5 mL tubes containing 3.2% citrate (BD, Plymouth, UK). To prepare RBCs, we centrifuged blood at 3500 × g for 10 min at 4 °C. Isolated RBCs were then mixed with PBS and added to the HUVECs (plated on transwell membranes) that had been treated with APL/NB4-CM for 24 h as previously described. After 15 min, the number of leaked RBCs was measured using a blood cell counting chamber.

2.7. Measurement of serum sVCAM-1, sICAM-1, sE-selectin and sTM levels

Following 24 h of APL/NB4-cell treatment, ICAM-1 and VCAM-1 expression levels in HUVECs were quantified by Western blot analysis and densitometry using ImageJ software. Peripheral venous blood was drawn from APL patients and added to a 5 mL tube with 3.2% citrate. To obtain serum, blood was treated as centrifugation at 3600r for 15 min at 4 °C. The serum sVCAM-1, sICAM-1, sTM, and sE-selectin concentrations of patients were quantified using the corresponding ELISA kits.

2.8. Scanning electron microscopy (SEM) of the plasma fibrin network

NB4/APL-treated HUVECs on coverslips were incubated with citrated plasma for 24 h with $CaCl_2$ (25 mmol/L). Then, samples were washed with PBS 3 times and fixed with glutaraldehyde. Na-cacodylate HCl buffer (0.1 M) was used to rinse the samples, and 1% OsO_4 was used to postfix the samples. Then, the samples were dehydrated twice for 5 min each in the following graded ethanol series: 30%, 50%, 70%, 90%, and 100%. After drying, the samples were covered by a 10-nm-thick platinum layer. All images were obtained using an S-3400 N electron microscope (Hitachi Ltd.) in ultrahigh-resolution mode. The density of fibrin networks was calculated by measuring the percentage of the fiber area of the total image area. To quantify the openings within the endothelial layer, gaps were regarded as a circle, and then we estimated the diameters (d) from measured areas as previously described [24]. Two hundred gaps were measured from 10 images.

2.9. Confocal microscopy

Structural changes in HUVECs were observed by staining with anti-VE-cadherin-Alexa Fluor 488 and TRITC-phalloidin**.** PS exposure on the surface of HUVECs was detected by incubation with lactadherin-Alexa Fluor 488 and FITC-annexin V for 10 min in the dark. FXa and FVa binding images were obtained by co-staining stimulated HUVECs with fluorescein-labeled FVa- and EGRckbiotin-labelled FXa. Fbg conjugated to Alexa Fluor 647 and lactadherin labeled with Alexa Fluor 488 were used to observe the fibrin network formed in stimulated HUVECs. The 488 or 568 nm emission lines of a krypton-argon laser were used to excite all the samples. We used a Zeiss LSM 510 META confocal microscope to capture images.

2.10. Western blotting

The cells were mixed with Tris-HCl lysis buffer including 1% Triton X-100, and then protein extraction was performed. Next, a 10% SDS-acrylamide gel was used to separate the samples, which were then electrophoretically transferred to a PVDF membrane. Then, 10% of non-fat milk was used to block the membrane, which was then washed and probed with anti-VE-cadherin, anti-ZO-1, anti-VCAM-1, anti-ICAM-1, and anti-β-actin antibodies. After washing, the membrane was incubated with an anti-mouse antibody conjugated with horseradish peroxidase. Visualization was performed using enhanced chemiluminescence plus (Pierce) according to the manufacturer's instructions.

2.11. Coagulation time and inhibition assays

The procoagulant activity of APL/NB4 cell-treated HUVECs was assessed by a one-stage recalcification time assay in a KC4A-coagulometer (Amelung, Labcon, Heppenheim, Germany). Fibrin formation on APL cells was quantified by turbidity assays. Briefly, 100 μL of experimental ECs (1 × 10^6) was resuspended in Tyrode's buffer (10 μL EC suspension + 90 μL Tyrode's buffer each well). The whole system was incubated with prewarmed microparticle-depleted plasma at 37 °C for 3 min. Then, 25 mM $CaCl_2$ (100 μL) was added and the time for fibrin formation was measured immediately. For inhibition assays, experimental ECs were pretreated with lactadherin (128 nM) or anti-TF (40 mg/mL) before the assay.

2.12. Experimental animals

Forty male or female SCID mice, aged 5–7 weeks, were obtained from Beijing Vital River Laboratory Animal Technology Co. Ltd. All animal procedures were conducted in the animal facility of the Animal Experimental Center of The Key Laboratory of Myocardial Ischemia complying with the Animal Care and Use Committee approved protocol. The mice were bred in sterilized cages and provided with a standard powdered rodent diet ad libitum and autoclaved water at 25 °C, 40%–70% humidity. Experimental protocols were initiated after a week acclimatization period. Then SCID mice were randomly divided into three groups (ten mice per group).

2.13. Cell apoptosis assay

We washed experimental cells were with PBS, then resuspended them in binding buffer. Lactadherin-FITC was used to stain with for 15 min to perform apoptosis assay. Fluorescence was measured using a flow cytometer. Apoptosis was identified by Lactadherin-FITC apoptosis detection kit from BD Pharmingen (San Diego, USA), complying with the manufacturer's instructions. FACScan flow cytometer combined with CELLQuest software (Becton Dickinson, Franklin Lakes, USA) was used to analyze prepared cells. To perform TUNEL (terminal deoxynucleotidyl transferase-mediated deoxyuridine triphosphate nick-end labeling) assay was performed as the previous descript.[1]

2.14. In vivo xenograft model

APL xenograft model was obtained using intravenous (i.v.) inoculation of exponentially growing NB4 cells (5×10^6/mouse) in SCID mice. Our lab established a xenograft tumor model using the NB4 cell line in SCID mice in our previous studies [25]. Tumors were visible at 14 days after mice were treated with NB4 cells. Then we observed xenograft mice began show following performance: the appearance of typical symptoms: wrinkled fur, less activity, depression, arch position, cornering or circling, gait instability, multiple lymphadenopathies, loss of appetite, thin and limb paralysis and specific APL cells markers' detection in the peripheral blood cells.

2.15. Secondary transplantation experiments

In all, 5×10^6 NB4 cells were injected into 6–8-weeks old SCID mice. On day 28, the mice were sacrificed and 1×10^7 bone marrow cells were transplanted into a new batch of 6–8-weeks-old mice. These new APL model mice were randomly separated into four groups and were treated with placebo, asiatic acid, anti-ICAM-1, and anti-VCAM-1 antibodies, respectively. In aisatic acid groups, the mice were orally administered with aisatic acid (10 mg/kg) for three weeks followed by UVR treatment for 24 h. In another two groups, the animals were intravenously injected with anti-ICAM-1 and anti-VCAM-1 antibodies (4 mg/kg) 30 min before the UVR treatment.

2.16. Creation of wound

After mice were anesthetized with 2% isoflurane, the dorsal skin of the mouse was shaved and cleaned with 75% alcohol. Using a marker pen to mark a 1 cm^2 area on the midline of the back. Then, a fine scissor was used to excise full-thickness skin. The progression of wound healing in all mice was analyzed every day.

2.17. Mice bleeding time

The experimental mice were treated with ATRA (5 mg/kg), ATO (5 mg/kg), ATRA +ATO, ATRA+Asiatic acid, ATO+Asiatic acid or ATRA +ATO + Asiatic acid for 21 days. Anesthetized animals' tails were amputated at 3 mm from the tip, after which bleeding time was measured as previously reported.

2.18. Statistical analysis

All data were analyzed by GraphPad Prism 7.0 or SPSS 16.0 statistical software. The mean ± standard deviation (SD) is used to present all of the results. Each result was collected from at least three independent experiments. Categorical variables were compared using the Chi-square test, and the Mann-Whitney U test was conducted for the nonparametric variable. Numerical variables were tested for normal distribution with the Kolmogorov Smirnov test. A paired *t*-test or ANOVA was used for analysis as appropriate, and a value of $P<0.05$ was considered statistically significant.

2.19. Funding sources

This work was supported by grants from the National Science Foundation of China (81470301, 81670128, 81873433). The funding organizations had no input in the design of the study; in the collection, analyses, or interpretation of the data; writing of the manuscript; or in the decision to submit the study for publication.

3. Results

3.1. Effect of leukaemic cells on endothelial barrier integrity

After 24 h of incubation with NB4/APL cells, ECs developed a spindle-shaped phenotype (Figure S1). Then, we incubated the endothelial monolayers with HL-60 cells, THP-1 cells, and AML-4 cells. None of these cells induced significant morphological changes in ECs (Fig. 1a). To further analyze the characteristics of endothelial integrity, the expression of junction protein vascular endothelial (VE)-cadherin and ZO-1 was examined, which showed that both VE-cadherin and ZO-1 expression were reduced in NB4/APL cell-treated ECs. Asiatic acid (30 μM, 6 h pretreatment), a cytoskeleton stabilizer, inhibited the loss of junction protein expression (Fig. 1b-e). VE-cadherin localization at the cell membrane was sporadic and internalized, peripheral F-actin reorganized and formed a stress fiber pattern, and EC borders were retracted resulting in gaps in the target group (Fig. 1f). Upon treatment with NB4 medium supernatant alone, the retracted cells nearly returned to normal within 6 h, and junction proteins remained attached (Fig. 1g). Next, a transendothelial albumin passage test was performed to analyze endothelial integrity at a functional level. The permeability of APL cell-treated EC monolayers to albumin progressively increased and peaked at 16 h with more than a 3-fold higher protein flux than that of the control. The inflection points of the permeability curve occurred at 8 h. Pretreatment with asiatic acid significantly attenuated the hyperpermeability induced by APL cells (Fig. 1h). Taken together, leukaemic cells alone induce abnormal endothelial actin-myosin distribution, which disrupts endothelial integrity and increases endothelial permeability.

3.2. HUVEC permeability to RBCs increases in response to APL cells

After APL cell treatment, ECs detached from each other by 4 h, with VE-cadherin loss and increased gap sizes observed after 4 to 12 h. In the asiatic acid group, most ECs were still attached at 4 h after leukaemic cell incubation, and smaller gaps were observed by 16 h (Fig. 2a). Then, the gaps were approximated as circles, and the diameter was measured using SEM. Approximately 60% of the gaps ranged from 10 to 15 μm in the leukaemic cell groups, enabling both mature (6 μm) and nucleated (8 μm) RBCs to pass through. The percentage of these large gaps was significantly decreased by pre-treatment with asiatic acid (Fig. 2b, c). Next, a transendothelial RBCs passage assay was performed (Fig. 2d). The untreated endothelial monolayers

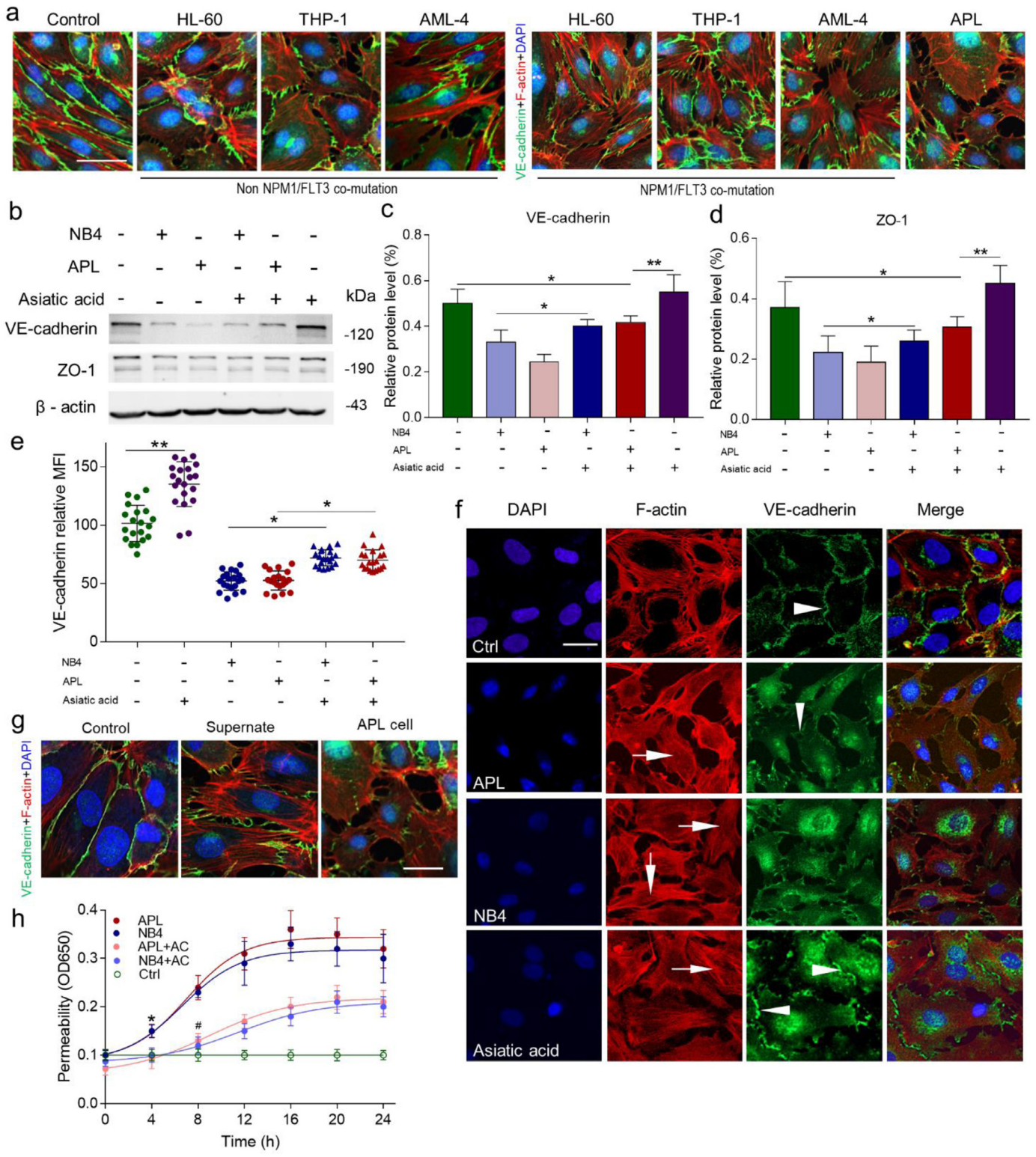

Fig. 1. Effect of NB4/APL-CM on HUVEC structure and morphology. (A) Endothelial monolayers were incubated with RPMI 1640 medium, HL-60, THP-1, AML-4, and APL cells for 24 h. Confocal microscopy was used to image. DAPI (blue) and F-actin (red) and VE-cadherin (green). The scale bar represents 20 μm. (B) HUVECs with/out pre-treatment with asiatic acid were incubated with APL/NB4 cells for 24 h. ZO-1 and VE-cadherin protein levels (β-actin as the loading control) were imaged by western blot analysis with the respective antibodies after 24 h of incubation. (C, D) The protein levels of ZO-1 and VE-cadherin relative to those of β-actin in (A) were assessed using ImageJ. (E) HUVECs were treated as described in (A). The expression of VE-cadherin on the endothelial membrane was measured by flow cytometry (expressed as the mean fluorescence intensity [MFI]). (F) Confocal microscopy showing that stimulated HUVECs retract, causing intercellular gaps. HUVECs were treated with NB4/APL cell medium or RPMI 1640 medium for 24 h, followed by co-staining with DAPI (blue) and F-actin (red) and VE-cadherin (green) antibodies. Asiatic acid (30 μM) stabilizes peripheral F-actin during APL cell incubation. Arrows point to stress fibers formed in the middle of the cell membrane, and arrowheads represent endothelial intercellular junction proteins. (G) EC monolayers were incubated with culture medium, APL cell culture medium supernatants alone, and APL cells. Images representative of 5 independent experiments are shown. The scale bar represents 20 μm. (H) HUVECs were incubated with NB4/APL cells or RPMI 1640 medium as a control for the indicated amounts of time, and permeability was measured as described in the "Methods" section. The graph is presented as the mean ± SD of at least five experiments. $^{*}P$ <0.05 and $^{**}P$ <0.01, $^{\#}P$ <0.05 vs. control group in panel H. (For interpretation of the references to color in this figure legend, the reader is referred to the web version of this article.)

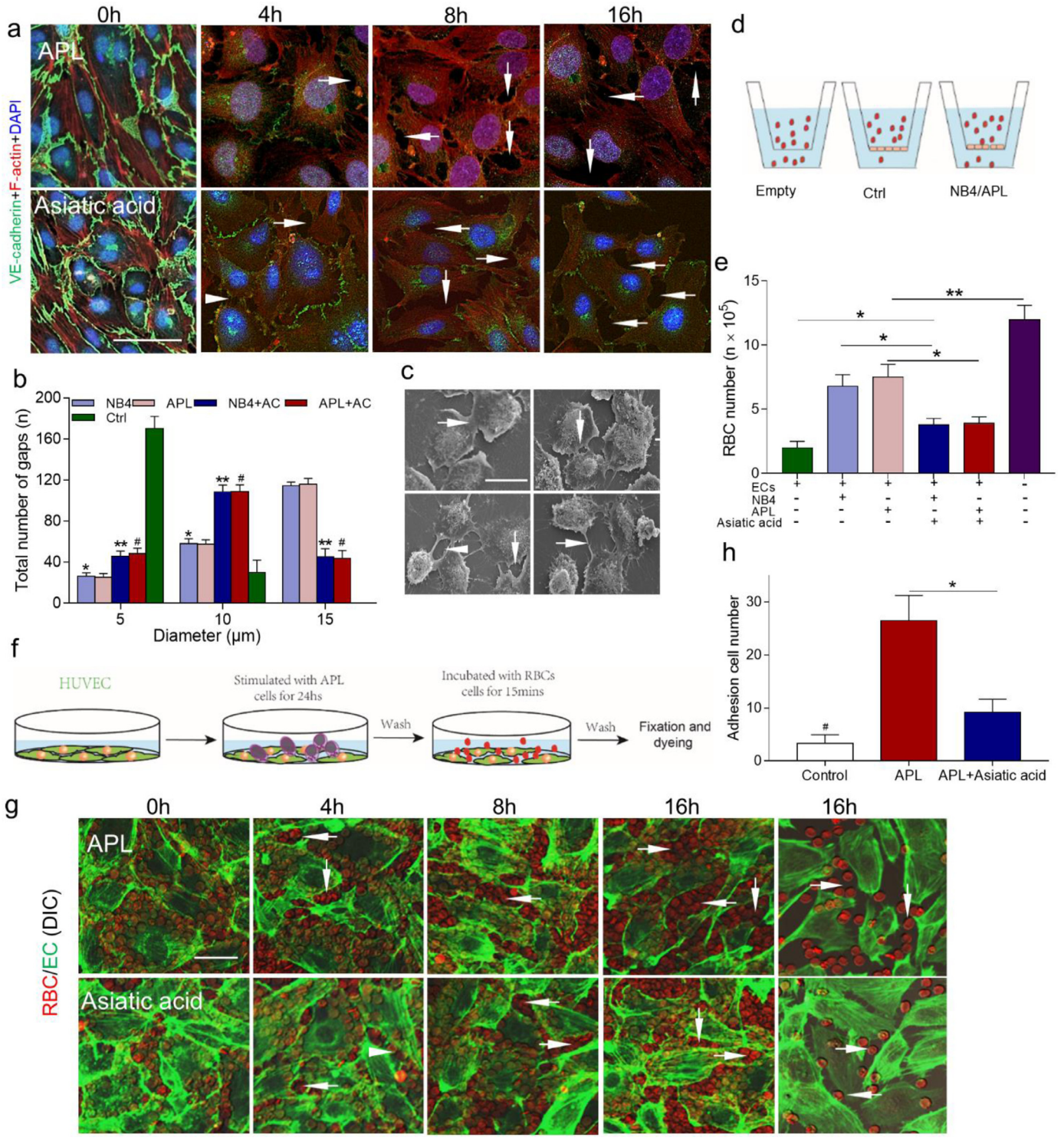

Fig. 2. RBCs pass through the damaged endothelium. (A) Confocal images showing changes in the HUVEC monolayer after treatment with APL-CM for 0, 4, 8, and 16 h (upper row). The HUVEC monolayer was pretreated with asiatic acid and induced with APL cell medium (lower row). The monolayer was stained with DAPI (blue) and for VE-cadherin (green) and F-actin (red). Arrows indicate gaps. Images representative of 3 independent experiments are shown. (B) The size distribution of the intercellular gaps induced by different levels of HUVEC stimulation; n = 200 gaps from 10 glass coverslips. (C) Electron micrographs showing different sized gaps (arrows) after 24 h of NB4/APL cell medium treatment. The upper panels show tight connections (left) and a gap of diameter 3.63 μm (right); the lower panels show gaps of 6.01 μm (left) and 14.14 μm (right). (D) Schematic representation of the RBC leakage experiment. (E) The number of leaked RBCs after endothelial monolayer incubation with RBCs. (F) Experimental scheme for RBC deposition. The HUVEC monolayer was pretreated with APL cells for 24 h to induce junction breakage. As the gaps grew in size and number, an increased area was exposed to which the RBCs could adhere. (G) RBCs (red) adhered to openings within endothelial monolayer treated as in (A). Arrows point to the RBCs deposited in the gaps. (H) The number of RBCs adhesion to the gaps at 16 h. Scale bars represent 20 μm in panels A, C, and G. The results indicate the mean ± SD of at least five experiments. $^{*}P$ <0.05 vs. the control group, $^{**}P$ <0.01 vs. the NB4 group, and $^{\#}P$ <0.05 vs. the APL group in panel B. $^{*}P$ <0.01, $^{**}P$ <0.001 in panel E, $^{*}P$ <0.05 in panel H. (For interpretation of the references to color in this figure legend, the reader is referred to the web version of this article.)

allowed 1.6 ± 0.3 × 10^5/mL RBCs to permeate. Incubation with NB4 or APL cells increased the RBC permeability values to 6.1 ± 0.4 × 10^5/mL and 7 ± 0.4 × 10^5/mL, respectively. However, the permeability was decreased to 3.8 ± 0.4 × 10^5/mL in both cell types in the presence of asiatic acid (Fig. 2d, e). Visually, all RBCs floated over the endothelium due to the lack of attachment area at 0 h. After APL cell stimulation, RBCs began to deposit in the gaps by 4 h (Fig. 2g). Compared to APL cells alone, pre-treatment with asiatic acid reduced the number of attached RBCs by ~3-fold (Fig. 2h). Therefore, endothelial gaps induced by APL cells are large enough for RBC extravasation, and this leakage could also be inhibited by asiatic acid.

3.3. RBC leakage depends on APL cell-endothelial interaction

Next, we aimed to find out how APL cells damage ECs. In this study, the expression levels of ICAM-1 and VCAM-1 were evaluated after 4 h of incubation with APL cells (Fig. 3a, b). Because we found that leukaemic cells themselves, but not their production, induced large and lasting gap formation, we sought to prevent RBC extravasation by inhibiting APL cell adhesion. Combined treatment with anti-ICAM-1 and anti-VCAM-1 antibodies resulted in reduced large gap formation and less RBC deposition than observed in the APL cell alone group (Fig. 3c). Interference with adhesion receptors led to

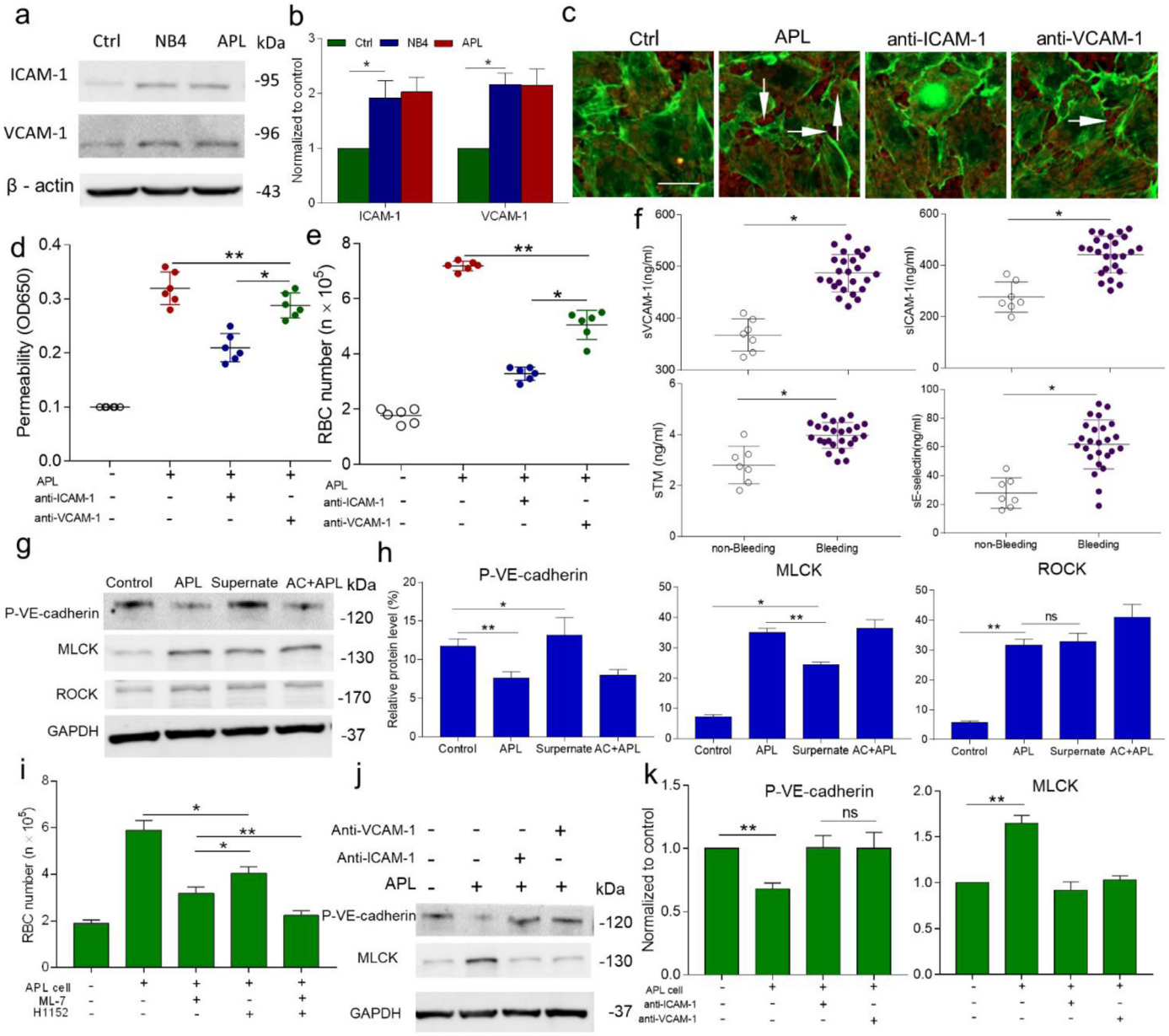

Fig. 3. APL cells adhere to ECs, causing impaired barrier function in vitro and in vivo. (A, B) The effect of APL/NB4 cells on ICAM-1 and VCAM-1 expression in HUVECs. Western blots were imaged, and the optical density was calculated using ImageJ. (C) ECs were stained with phalloidin, and RBCs were labeled with live-cell dye. Gap formation in the damaged endothelium permits RBC deposition (arrows). (D) The albumin permeability of the experimental monolayers treated with an adherence receptor antibody. (E) The permeability to RBCs upon treatment with an adherence receptor antibody. (F) The levels of sVCAM-1, sICAM-1, sE-selectin, and sTM in serum samples from the bleeding patient (open circles) and non-bleeding patient (closed circles) groups. (G) Western blotting with an anti-pVE-cadherin antibody, an anti-MLCK, and an anti-ROCK antibody for ECs treated with leukemic cells or supernatant alone. (H) Quantitation of the relative protein expression level in (G) by ImageJ (Gapdh was used as the loading control). (I) Pretreatment with MLCK inhibitor ML-7 (10^{-4} mol/L) or/and with ROCK inhibitor H1152 (2.5 μmol) for 1 h, then incubated with APL cells for 16 h. Permeability of treated endothelium to RBCs. (J) Expression of pVE-cadherin and MLCK in ECs treated with anti-ICAM-1 and anti-VCAM-1 antibodies, respectively, was assayed by western blotting and compared with that in the control and APL samples. (K) Quantitation of the relative protein expression level in (J) by ImageJ. The inset bar represents 20 μm in panel F. AC+APL: Asiatic acid + APL cells. The graph is presented as the mean ± SD of at least five experiments. $^*P$ <0.05 and $^{**}P$ <0.01.

significantly decreased albumin leakage and RBC extravasation (Fig. 3d, e). Moreover, the inhibitory effect of anti-ICAM-1 antibodies was greater than that of anti-VCAM-1 antibodies. The ex vivo results confirmed that compared to non-bleeding patients, patients who experienced bleeding within 24 h of diagnosis showed increased EC dysfunction marker expression including sICAM-1, sVCAM-1, sTM, and sE-selectin (Fig. 3f).

To investigate the specific mechanism through which APL cells induced large endothelial gap formation, we assessed the expression levels of two critical mediators of EC contraction. Increased ROCK expression was observed in both the leukaemia cell and supernatant groups. However, increased expression of MLCK and induction of reduced pVE-cadherin expression were only found in the presence of APL cells (Fig. 3g, h). At the functional level, the MLCK inhibitor ML-7 significantly reduced endothelial permeability to proteins and the number of leaked RBCs compared to the APL cell group (Fig. S3, Fig. 3i). Anti-ICAM-1 and anti-VCAM-1 antibodies reduced MLCK expression, and increased levels of pVE-cadherin were observed (Fig. 3j, k).

3.4. ATRA represses the effect of NB4 cells on ECs by stabilizing EC activity

With the routine incorporation of ATRA and ATO into the clinical practice, we sought to explore their role in endothelial monolayers in this study. In contrast to ATO, ATRA reversed EC retraction and induced contact in dissociated ECs. However, exposure to ATO increased the loss of junction protein. The decreased expression of VE-cadherin furthermore coincided with worse EC-cell contact (Fig. 4a). In the presence of ATRA, the transendothelial passage of

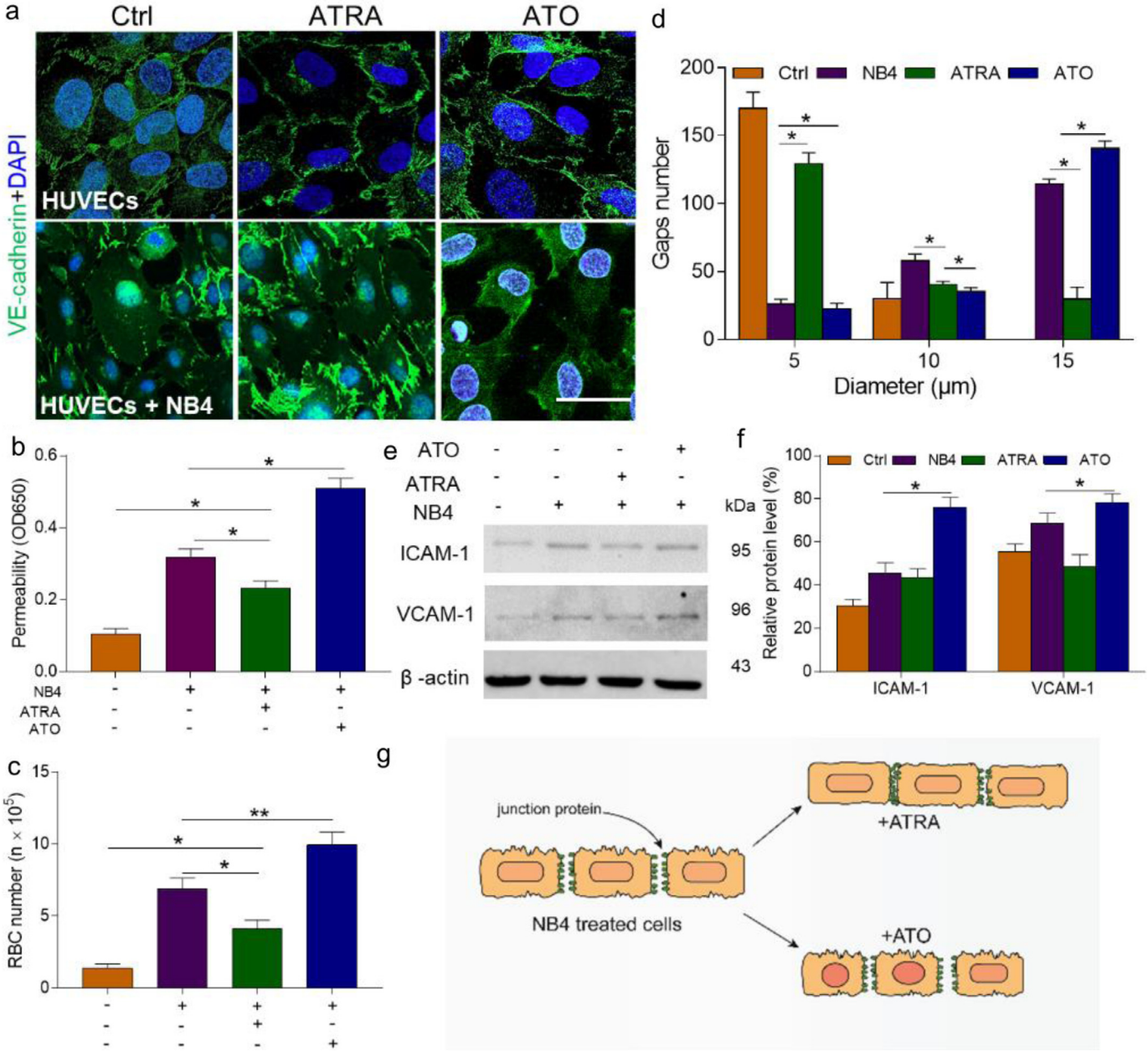

Fig. 4. ATRA protects HUVEC barrier function. (A) A laser confocal microscope was used to image the changes in the junction protein VE-cadherin (green) and DAPI (blue) staining. The inset bar represents 10 μm. (B) The permeability of NB4-treated HUVECs incubated with or without ATRA (1 μmol/L) or ATO (5 μmol/L) was tested as previously described. (C) The number of leaked RBCs was measured as previously described. (D) The distribution of intercellular gap size was improved by ATRA treatment of the target HUVECs; n = 200 gaps from 10 glass coverslips. (E, F) Effect of ATRA and ATO on ICAM-1 and VCAM-1 concentrations. (G) Schematic illustration of the effect of ATRA and ATO on NB4-treated HUVECs. ATRA protects NB4-treated HUVECs, whereas ATO worsens the damage. $^{*}P$ <0.05 and $^{**}P$ <0.01. The results are displayed as the mean ± SD from at least 6 experiments. (For interpretation of the references to color in this figure legend, the reader is referred to the web version of this article.)

albumin and the amount of RBC extravasation were reduced by 41% and 48%, respectively; in the presence of ATO, these values were increased by 61% and 47% (Fig. 4b, c). Then, we measured the size of the gaps in the ATRA- and ATO-treated monolayers. We found that 64.7% of openings measured in the ATRA group were smaller than an RBC (5 μm or less in diameter). In contrast, 70% of the gaps in the ATO group were much larger than the diameter of an RBC (Fig. 4d). Combined treatment with ATO produced more gaps than treatment with NB4 cells alone (57%). Additionally, the expression levels of ICAM-1 and VCAM-1 were also reduced by ATRA (Fig. 4e). Therefore, ATRA inhibited the transendothelial passage of RBCs by recovering EC junction protein as well as decreasing the expression of adhesion receptors.

3.5. Endothelial damage contributes to bleeding in the APL model

Further experiments were performed in an APL mouse model. SCID mice were transplanted with NB4 cells and were monitored until they exhibited signs of leukaemia (Figure S4). At 21 days after implantation, the ICAM-1 and VCAM-1 levels in the peripheral blood of APL mice were elevated. Asiatic acid decreased the concentration of both proteins (Fig. 5a, b). Dorsal microvasculature exposure to UV

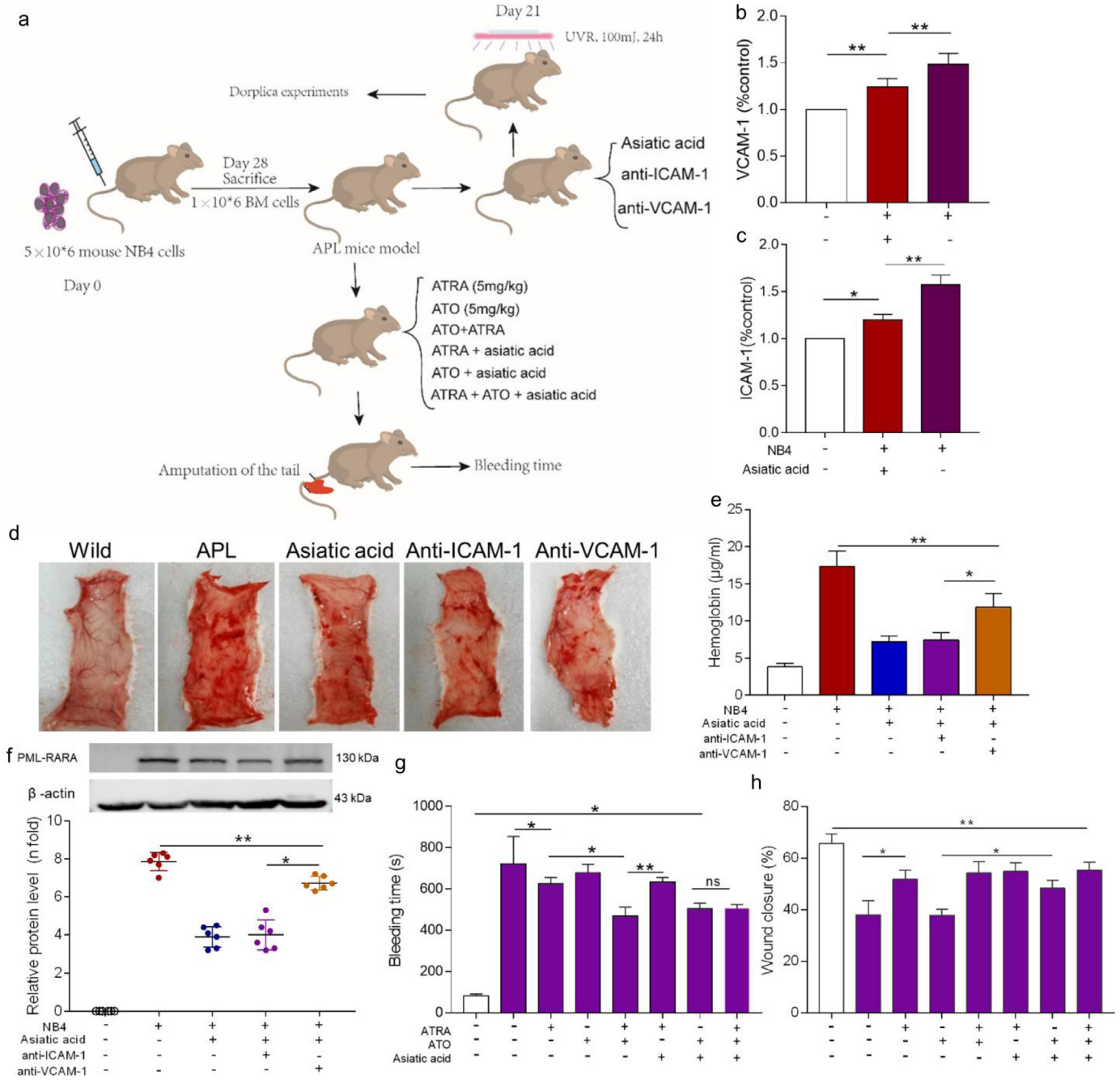

Fig. 5. Asiatic acid alleviates bleeding in the APL model. (A) The outline depicts the transplantation experiments. Dorplica experiments mean the back skin of the mice was cut off to observe subcutaneous bleeding. (B, C) The levels of sICAM-1 and sVCAM-1 were measured in mouse serum samples collected from the caudal vein. (D) Representative images of prepared back skins of the APL model mice with different treatments and 24 h of UV light exposure. (E) Analysis of the hemoglobin concentration in the bleeding spots. (F) The expression of PML-RARA protein in the areas of bleeding. (G) The bleeding time was tested as previously described. (H) Wound closure of APL model mice one week after injury. The white columns represent the data of mice that have not received leukemic cells, the purple columns represent the data of mice that received leukemic cells. $^{*}P < 0.05$, $^{**}P < 0.01$, ns, nonsignificant. The results are shown as the mean ± SD of at least 3 experiments.

light induces aseptic inflammation with increased levels of ICAM-1 and VCAM-1 expression [26]. Therefore, wild-type mice and APL model mice were intravenously treated with asiatic acid or anti-ICAM-1 or VCAM-1 antibodies and exposed to UV light for 24 h. Severe petechial bleeding was found in the APL group and the anti-VCAM-1 group. Combined treatment with asiatic acid or an anti-ICAM-1 antibody effectively alleviated bleeding, and no bleeding spots were observed in wild-type mice (Fig. 5d, e). Tissue infiltration analysis via the PML-RARA expression level showed significant APL cell accumulation at bleeding sites (Fig. 5f). Animals treated with ATO plus asiatic acid or ATRA showed markedly shortened bleeding time and reduced wound healing time compared to those treated with ATRA and asiatic acid (Fig. 5g, h). Therefore, these results suggest that asiatic acid both prevents leukaemic cell adhesion and protects ECs, thereby inhibiting APL-induced bleeding in vivo.

3.6. Fibrin network formation between procoagulant ECs compensates for the compromised permeability in vitro

In response to APL cells, the percentage of PS exposure in ECs increased progressively (Fig. 6a). Because exposure PS is the main mechanism that promotes procoagulant activity in blood cells and

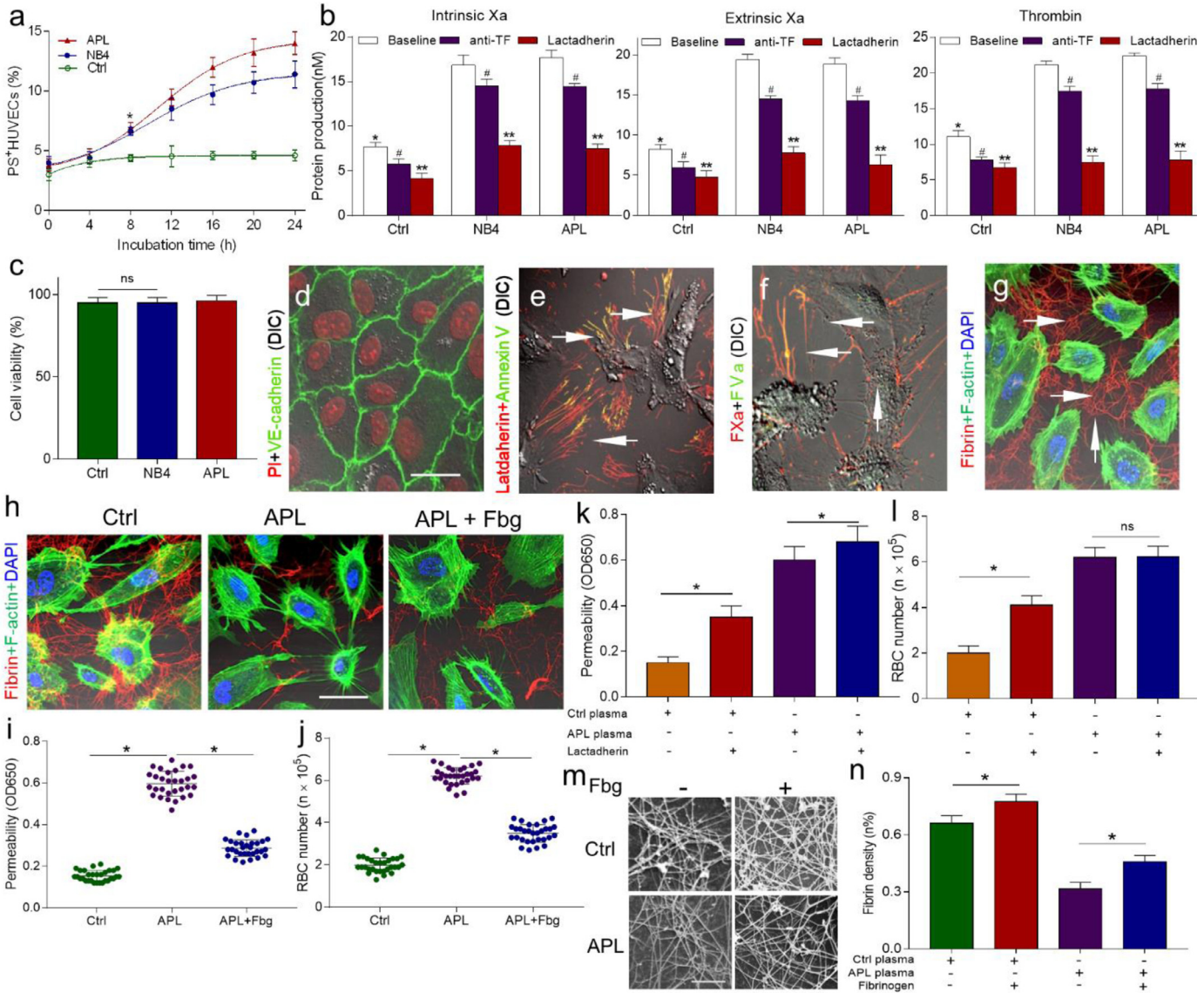

Fig. 6. Intercellular fibrin networks compensate for the damaged barrier function. (A) The kinetics of PS exposure on HUVECs treated with APL cells were measured using lactadherin labeling and flow cytometry. (B) For the inhibition assays, APL-treated HUVECs were preincubated with lactadherin (128 nM) or an anti-TF antibody (40 μg/mL), and the coagulation proteins - intrinsic Xa, extrinsic Xa and thrombin (from left to right) were measured. (C) After treated with APL/NB4 cells, EC viability was analyzed by trypan blue exclusion. (D) Control HUVECs cultured with RPMI 1640 medium and stained with propidium iodide (PI; red) and VE-cadherin (green). (E) HUVECs treated with patient APL cells stained with lactadherin (red) and FITC-annexin V (green) for PS exposure. (F) Filopodia (arrows) of retracted ECs were co-stained (yellow) with FXa (red) and FVa (green). (G) HUVECs treated with APL cells displayed fibrin network production along the filopodia (arrows) after incubated with healthy volunteers' plasma. Four images (D-G) were obtained by confocal microscopy. The scale bars in panels D-G represent 5 μm. (H) Recalcified healthy or APL patient plasma was applied over NB4-treated HUVEC monolayers, stained for fibrin (red) and F-actin (green) and with DAPI (blue), and then imaged using confocal microscopy. (I) The albumin permeability of each sample was tested after 15 min. (J) The number of leaked RBCs in each sample prepared as described in (I). (K) The albumin permeability of the experimental monolayers with/without lactadherin (128 nM). (L) The number of leaked RBCs was measured as in (K). (M) APL-treated HUVECs (16 h time point) were incubated with plasma from healthy volunteers and APL patients with/without fibrinogen (1 g/L). The fibrin network of the samples was observed by a scanning electron microscope. Each image comes from 1 experiment and represents at least three experiments. The scale bar represents 10 μm. (N) The mean density of the fibrin network was calculated using ImageJ software. $^{*}P < 0.05$ vs. the baseline in the NB4 group, $^{\#}P < 0.05$ vs. the baseline, $^{**}P < 0.01$ vs. the anti-TF group in panels A and B. Every graph indicates the mean ± SD from at least five experiments. Ctrl, control group; APL, APL patient group; APL+Fbg, APL patient group + Fbg. (For interpretation of the references to color in this figure legend, the reader is referred to the web version of this article.)

Table 2
Fibrin network density with different doses of additional Fbg.

Fbg dose(g/l)	0	0.5	1.0	1.5	2.0
Control (%)	65 ± 3.9*	72 ± 3.6*	76 ± 2.5*	80 ± 2.4*	80 ± 2.4*
APL (%)	34 ± 1.7	38 ± 2**	45 ± 1.8**	52 ± 1.1**	54 ± 2**

The density of fibrin networks was measured as described in the "Materials and methods". Each data point represents at least 6 experiments.
* $P < 0.05$ vs. the APL group,.
** $P < 0.01$ vs. the prior data in APL group.

microparticles [27,28], in this study, we decided to examine whether PS exposure in ECs leads to a procoagulant phenotype. An anti-TF antibody and lactadherin were used to perform inhibition experiments. Thrombin, intrinsic FXa, and extrinsic FXa activity were decreased by approximately 60%, in the presence of lactadherin. Compared to lactadherin, anti-TF antibodies inhibited approximately 13% of extrinsic FXa activity (Fig. 6b). The addition of lactadherin also resulted in a significantly prolonged coagulation time (Figure S5). Alexa Fluor 647-labeled lactadherin and Alexa Fluor 488-labelled Annexin V was observed on the filopodia of EC margins, showing PS externalization (Fig. 6e). Consistent with the coagulation results, FVa and FXa co-localized on the filopodia of ECs (Fig. 6f). Moreover, fibrin networks spread radially across gaps between filopodia (Fig. 6g). When leukaemic cell-treated endothelial monolayers were exposed to APL patient plasma with/without additional Fbg, we observed significantly increased intercellular fibrin density in the group with the addition of Fbg (Fig. 6h). Then, we examined whether intercellular fibrin networks support endothelial integrity. The addition of Fbg to the APL group samples decreased the rate of albumin permeability by 48.33% and the number of leaked RBCs by ~2-fold (Fig. 6i, j). Additionally, the barrier function of the intercellular network was inhibited by lactadherin, as affected the coagulation ability of ECs (Fig. 6k, l). Finally, we used SEM to directly observe the fibrin networks formed in target ECs. The addition of exogenous Fbg increased the clot density in both APL and control plasma in a dose-dependent manner (Fig. 6m, n, Table 2).

4. Discussion

We made four significant observations in this study. First, APL cells are the key players that trigger the endothelial retraction and pore formation, resulting in endothelial hyperpermeability and haemorrhage. Moreover, asiatic acid protected ECs from leukaemic cell activation and alleviated APL bleeding. Second, ATRA, but not ATO, rescued the morphological alterations of ECs that occur during exposure to NB4 cells. Third, APL cell-treated ECs convert to a procoagulant phenotype through PS exposure, which is the major cause of intercellular fibrin network formation. Fourth, fibrin networks along the edge of the retracted ECs function to seal the barrier injury and reduce the number of RBCs leaking out of the barrier (Fig. 7).

In the context of APL, ECs have been shown to contribute to haemorrhage via procoagulant activity [29]. However, no further analysis of the APL endothelial structure has been reported. The integrity of the endothelial barrier depends on the cooperation between actin dynamics and junctional remodeling [30]. In response to coincubation with APL cells, the actin cytoskeleton exhibited a stress fiber

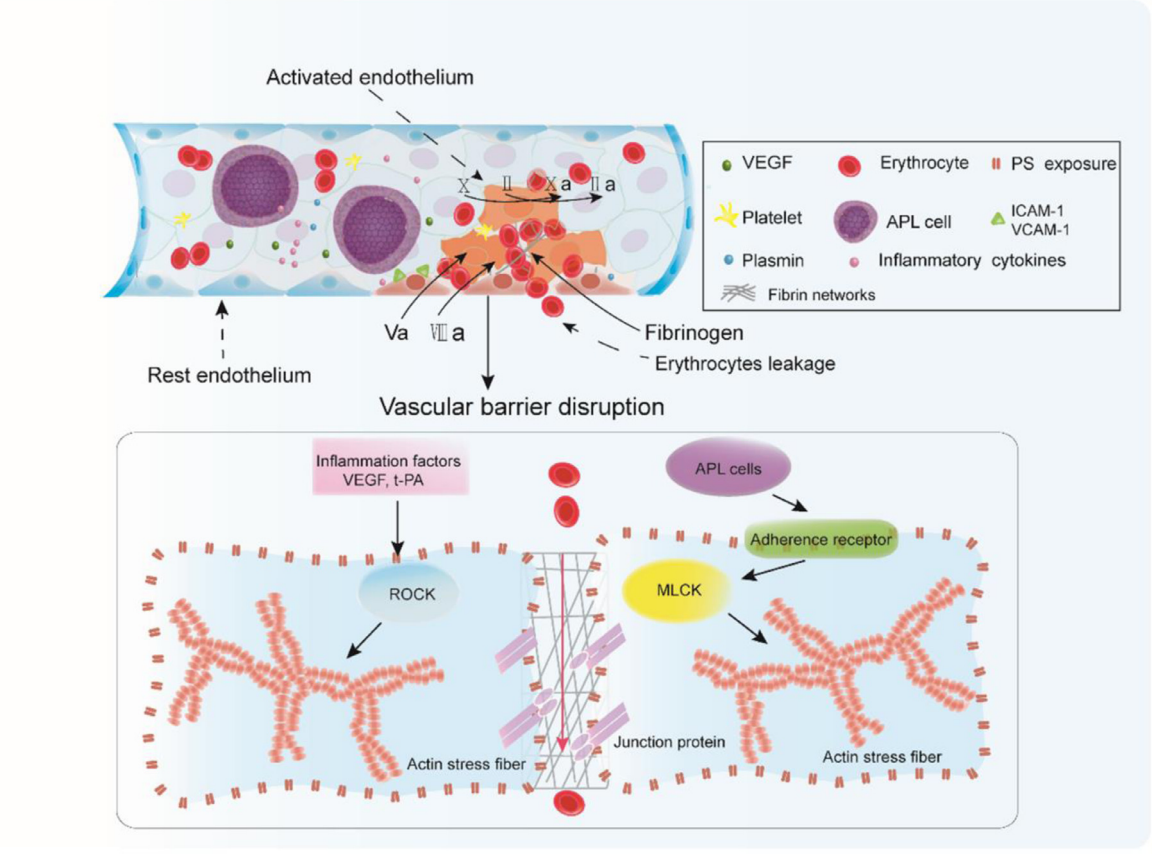

Fig. 7. Intercellular fibrin networks prevent erythrocyte leakage. VEGF, inflammatory cytokines, and APL blasts interact with ECs. Cellular factors activate ROCK signaling, whereas APL cells adhere to the adherence receptors ICAM-1 and VCAM-1 and trigger the MLCK pathway, resulting in stress fiber formation, EC retraction, and junction protein dissociation. The gaps among dissociated junctions are large enough to permit RBC transmigration. PS exposure on the activated ECs provides a catalytic surface for FV and FVIII, resulting in coagulation pathway activation and fibrin formation among the openings. Intercellular fibrin works to repair the integrity of the endothelium. Plasmin activated through the overexpression of t-PA from APL blasts acts to weaken the fibrin network, allowing RBCs to leak into the extravascular space.

pattern, leading to EC contraction and intercellular gap formation. Upon stabilization of F-actin distribution by asiatic acid, endothelial hyperpermeability and induction of RBC extravasation were significantly inhibited. These data indicate that endothelial contraction is needed for APL-induced haemorrhage. The endothelial barrier could have been disrupted by APL cells [24], inflammatory factors [31,32], or extracellular traps [21] in this study. Therefore, we examined which of these mechanisms was mainly responsible for the disruption of endothelial barrier integrity thus promoting haemorrhage. Endothelial contraction was reversed within 6 h when ECs were exposed to leukaemic cell medium supernatant alone. In addition, the intercellular gaps in the endothelium in this study were much larger than intercellular poles induced by inflammatory factors [33,34]. Thus, collectively, our results suggest that leukaemic cell-triggered endothelial contraction plays a major role in promoting haemorrhage in APL. These results are supported by previous studies [35,36].

APL blast adhesion to inflammatory factor-stimulated endothelium was dependent on ICAM-1 and VCAM-1 [37]. Interestingly, by interference with leukaemic cell adhesion, we could prevent APL mice from exhibiting inflammation-induced haemorrhage. ECs can be activated by many factors including IL-1β, TNF-α, the complement system, and extracellular DNA. However, the analysis of which these factors are mainly responsible for EC activation will be performed in a future study. Extensive analysis of leukaemic cell-EC binding has not been studied at the molecular level in previous studies. MLCK and ROCK are two critical mediators of EC contraction in physical and pathological conditions [38]. APL blasts specifically activated the MLCK pathway, resulting in RBC extravasation. However, ROCK signaling is also involved in the destruction of endothelial barrier integrity (Fig. 3). F-actin is a common downstream protein of these two molecules. Thus, it is reasonable that pretreatment with asiatic acid alone apparently reduced inflammatory haemorrhage in vivo. Additionally, a recent study reported the effect of asiatic acid on decreasing the inflammatory reaction in cancer [15]. Therefore, effects on vascular integrity may play a role in the beneficial effects of asiatic acid in patients with APL.

One interesting finding was the barrier-protective effect of intercellular fibrin networks, which prevented RBC extravasation. This protective function was regulated by the Fbg concentration and the extent of PS exposure in ECs. Available datasets have reported the importance of fibrin polymerization and thrombin generation for clot formation. However, we showed here that Fbg addition alone significantly contributed to clotting in APL patients (Figure S6). Moreover, Fbg addition increased the barrier function of intercellular fibrin networks in a concentration-dependent manner because Fbg is the decisive factor for clot structure [39]. In summary, additional Fbg not only supports the barrier function of intercellular fibrin but also improves clot structure in APL patients. Additionally, compared to other blood products, in terms of bleeding prevention, Fbg acts as both a procoagulant molecule and a protector of vascular integrity. Platelets also interact with ECs to safeguard vascular integrity [17]. However, in microvascular bleeding, platelets almost exclusively compose haemostatic plugs [40]. In this regard, intercellular fibrin may have the ability to maintain vascular integrity. Additionally, Fbg supplementation results in a better profile than platelet supplementation in clinical practice [41,42]. TF has been regarded as a major source of EC procoagulant activity in APL coagulopathy, although little has been reported about the involvement of PS exposure. However, in our study, coagulation assays and inhibition experiments showed that PS exposure of leukaemic cell-treated ECs was the main source of excessive EC procoagulant activity in APL coagulopathy. One possibility is that plasma-TF activity is increased upon PS exposure [43]. Moreover, the procoagulant activity induced by PS exposure supports intercellular fibrin formation. These results suggest that PS exposure is also a necessary component of this barrier function. In haemorrhage, PS exposure of injured ECs occurs before platelet aggregation [44]. Thus, exposure of ECs to PS appears to have a dual effect in APL haemorrhage.

ATRA and ATO are best known as differentiating agents in the treatment of APL. They decrease the incidence of APL-induced haemorrhage via reducing the procoagulant activity and hyperfibrinolysis-promoting properties of APL cells [45]. However, our findings provide a new mechanism for ATRA to counteract APL haemorrhage. ATRA directly reversed EC contraction and increased junction protein expression in this study. Consequently, the number of leaked RBCs and the transmigration of albumin were significantly decreased (Fig. 4). Thus, this barrier-restoring effect of ATRA is involved in preventing haemorrhage in APL. Other studies support our conclusion [46,47]. Strikingly, although ATO showed the opposite effect and induced apoptosis of target ECs, combined treatment with ATO and asiatic acid was able to protect APL mice from inflammation-induced haemorrhage. Conversely, treatment with ATRA combined with asiatic acid did not exhibit a similar effect. One explanation is that asiatic acid blocks the oxidative stress induced by ATO in vascular ECs [48,15]; consequently, the activation or apoptosis of ECs is inhibited. Another possibility is that ATO caused more apoptosis in APL cells [49]. Therefore, our results provide new insight into APL therapy.

In summary, this study reveals the mechanisms through which APL cells trigger endothelial barrier function breakdown. Endothelial contraction contributes in part to APL-induced haemorrhage. Intercellular fibrin networks, acting as a complementary barrier, bolster endothelial integrity in an Fbg dose-dependent manner. These findings provide potential insights into therapy improvements, although the supportive measures recommended to treat coagulopathy have not changed during the past decade [50]. Additionally, approximately 60% of APL patients with bleeding who are on induction and supportive therapy did not receive the recommended amount of Fbg [51]. Thus, reassessment of the target level of transfused Fbg according to different risk stratifications may also be necessary.

Declaration of Competing Interest

The authors declare no competing financial interests.

Acknowledgments

The authors thank Yanming Xue, Jingdong Qu, Rui Huang for the sample collection, and Yufeng Liu, Lei Gao, Qiusheng Wang for excellent technical assistance.

Supplementary materials

Supplementary material associated with this article can be found, in the online version, at doi:10.1016/j.ebiom.2020.102992.

Reference

[1] Abaza Y, Kantarjian H, Garcia-Manero G, et al. Long-term outcome of acute promyelocytic leukemia treated with all-trans-retinoic acid, arsenic trioxide, and gemtuzumab. Blood 2017;129:1275–83.
[2] Lehmann S, Deneberg S, Antunovic P, et al. Early death rates remain high in high-risk APL: update from the Swedish Acute Leukemia Registry 1997-2013. Leukemia 2017;31:1457–9.
[3] Breccia M, Lo Coco F. Thrombo-hemorrhagic deaths in acute promyelocytic leukemia. Thromb Res 2014;133(Suppl 2):S112–6.
[4] Park JH, Qiao B, Panageas KS, et al. Early death rate in acute promyelocytic leukemia remains high despite all-trans retinoic acid. Blood 2011;118:1248–54.
[5] Breen KA, Grimwade D, Hunt BJ. The pathogenesis and management of the coagulopathy of acute promyelocytic leukaemia. Br J Haematol 2012;156:24–36.
[6] Kolev K, Longstaff C. Bleeding related to disturbed fibrinolysis. Br J Haematol 2016;175:12–23.
[7] Mantha S, Goldman DA, Devlin SM, et al. Determinants of fatal bleeding during induction therapy for acute promyelocytic leukemia in the ATRA era. Blood 2017;129:1763–7.

[8] Nachman RL, Rafii S. Platelets, petechiae, and preservation of the vascular wall. N Engl J Med 2008;359:1261–70.
[9] Privratsky JR, Paddock CM, Florey O, et al. Relative contribution of PECAM-1 adhesion and signaling to the maintenance of vascular integrity. J Cell Sci 2011;124:1477–85.
[10] Gautam J, Miner JH, Yao Y. Loss of Endothelial Laminin α5 Exacerbates Hemorrhagic Brain Injury. Transl Stroke Res 2019;10:705–18.
[11] Stroka KM, Aranda-Espinoza H. Endothelial cell substrate stiffness influences neutrophil transmigration via myosin light chain kinase-dependent cell contraction. Blood 2011;118:1632–40.
[12] Passaro D, Di Tullio A, Abarrategi A, et al. Increased vascular permeability in the bone marrow microenvironment contributes to disease progression and drug response in acute myeloid leukemia. Cancer Cell 2017;32:324–41.
[13] Hillgruber C, Pöppelmann B, Weishaupt C, et al. Blocking neutrophil diapedesis prevents hemorrhage during thrombocytopenia. J Exp Med 2015;212:1255–66.
[14] Wu Q, Lv T, Chen Y, et al. Apoptosisof HL-60 human leukemia cells induced by Asiatic acid through modulation of B-cell lymphoma 2 family proteins and the mitogen-activated protein kinase signaling pathway. Mol Med Rep 2015; 12:1429–34.
[15] Kong D, Fu P, Zhang Q, Ma X, Jiang P. Protective effects of Asiatic acid against pelvic inflammatory disease in rats. Exp Ther Med 2019;17:4687–92.
[16] Fong LY, Ng CT, Yong YK, Hakim MN, Ahmad Z. Asiatic acid stabilizes cytoskeletal proteins and prevents TNF-α-induced disorganization of cell-cell junctions in human aortic endothelial cells. Vascul Pharmacol 2019;117:15–26.
[17] Ho-Tin-Noé B, Boulaftali Y, Camerer E. Platelets and vascular integrity: how platelets prevent bleeding in inflammation. Blood 2018;131:277–88.
[18] Lee RH, Bergmeier W. Platelet immunoreceptor tyrosine-based activation motif (ITAM) and hemITAM signaling and vascular integrity in inflammation and development. J Thromb Haemost 2016;14:645–54.
[19] Velik-Salchner C, Haas T, Innerhofer P, et al. The effect of fibrinogen concentrates on thrombocytopenia. J Thromb Haemost 2007;5:1019–25.
[20] Schenk B, Lindner AK, Treichl B, et al. Fibrinogen supplementation ex vivo increases clot firmness comparable to platelet transfusion in thrombocytopenia. Br J Anaesth 2016;117:576–82.
[21] Cao M, Li T, He Z, et al. Promyelocytic extracellular chromatin exacerbates coagulation and fibrinolysis in acute promyelocytic leukemia. Blood 2017;129:1855–64.
[22] Liu Y, Li B, Hu TL, Zhang Y, Zhang C, Yu M, et al. Increased phosphatidylserine on blood cells in oral squamous cell carcinoma. J Dent Res 2019;98:763–71.
[23] Zhou J, Shi J, Hou J, et al. Phosphatidylserine exposure and procoagulant activity in acute promyelocytic leukemia. J Thromb Haemost 2010;8:773–82.
[24] Lavallée VP, Chagraoui J, MacRae T, et al. Transcriptomic landscape of acute promyelocytic leukemia reveals aberrant surface expression of the platelet aggregation agonist Podoplanin. Leukemia 2018;32:1349–57.
[25] Li T, Ma R, Zhang Y, et al. Arsenic trioxide promoting ETosis in acute promyelocytic leukemia through mTOR-regulated autophagy. Cell Death Dis 2018;9:75–89.
[26] Chung KY, Chang NS, Park YK, Lee KH. Effect of ultraviolet light on the expression of adhesion molecules and T lymphocyte adhesion to human dermal microvascular endothelial cells. Yonsei Med J 2002;43:165–74.
[27] Yu M, Li T, Li B, et al. Phosphatidylserine-exposing blood cells, microparticles and neutrophil extracellular traps increase procoagulant activity in patients with pancreatic cancer. Thromb Res 2020;188:5–16.
[28] Wang L, Bi Y, Yu M, et al. Phosphatidylserine-exposing blood cells and microparticles induce procoagulant activity in non-valvular atrial fibrillation. Int J Cardiol 2018;258:138–43.
[29] Kwaan HC, Cull EH. The coagulopathy in acute promyelocytic leukaemia—what have we learned in the past twenty years. Best Pract Res Clin Haematol 2014;27:11–8.
[30] García-Ponce A, Citalán-Madrid AF, Velázquez-Avila M, Vargas-Robles H, Schnoor M. The role of actin-binding proteins in the control of endothelial barrier integrity. Thromb Haemost 2015;113:20–36.
[31] Aveleira CA, Lin CM, Abcouwer SF, Ambrósio AF, Antonetti DA. TNF-α signals through PKCζ/NF-κB to alter the tight junction complex and increase retinal endothelial cell permeability. Diabetes 2010;59:2872–82.
[32] Komarova YA, Kruse K, Mehta D, Malik AB. Protein interactions at endothelial junctions and signaling mechanisms regulating endothelial permeability. Circ Res 2017;120:179–206.
[33] Baluk P, Hirata A, Thurston G. Endothelial gaps: time course of formation and closure in inflamed venules of rats. Am J Physiol 1997;272:L155–70.
[34] McDonald DM. Endothelial gaps and permeability of venules in rat tracheas exposed to inflammatory stimuli. Am J Physiol 1994;266:L61–83.
[35] Tornavaca O, Chia M, Dufton N, et al. ZO-1 controls endothelial adherens junctions, cell-cell tension, angiogenesis, and barrier formation. J Cell Biol 2015; 208:821–38.
[36] Marcos-Ramiro B, García-Weber D, Barroso S, et al. RhoB controls endothelial barrier recovery by inhibiting Rac1 trafficking to the cell border. J Cell Biol 2016;213:385–402.
[37] Stucki A, Rivier AS, Gikic M, et al. Endothelial cell activation by myeloblasts: molecular mechanisms of leukostasis and leukemic cell dissemination. Blood 2001;97:2121–9.
[38] Schnoor M, García Ponce A, Vadillo E, et al. Actin dynamics in the regulation of endothelial barrier functions and neutrophil recruitment during endotoxemia and sepsis. Cell Mol Life Sci 2017;74:1985–97.
[39] Domingues MM, Macrae FL, Duval C, et al. Thrombin and fibrinogen γ' impact clot structure by marked effects on intrafibrillar structure and protofibril packing. Blood 2016;127:487–95.
[40] Tomaiuolo M, Matzko CN, Poventud-Fuentes I, et al. Interrelationships between structure and function during the hemostatic response to injury. Proc Natl Acad Sci U S A 2019;116:2243–52.
[41] McCullough J. Current issues with platelet transfusion in patients with cancer. Semin Hematol 2000;37(2 Suppl 4):3–10.
[42] Blajchman MA. Incidence and significance of the bacterial contamination of blood components. Dev Biol (Basel) 2002;108:59–67.
[43] Bach RR. Tissue factor encryption. Arterioscler Thromb Vasc Biol 2006;26:456–61.
[44] Sakurai Y, Hardy ET, Ahn B, et al. A microengineered vascularized bleeding model that integrates the principal components of hemostasis. Nat Commun 2018; 9:509.
[45] O'Connell PA, Madureira PA, Berman JN, Liwski RS, Waisman DM. Regulation of S100A10 by the PML-RAR-α oncoprotein. Blood 2011;117:4095–105.
[46] Mizee MR, Wooldrik D, Lakeman KA, et al. Retinoic acid induces blood-brain barrier development. J Neurosci 2013;33:1660–71.
[47] Pal S, Iruela-Arispe ML, Harvey VS, et al. Retinoic acid selectively inhibits the vascular permeabilizing effect of VPF/VEGF, an early step in the angiogenic cascade. Microvasc Res 2000;60:112–20.
[48] Roboz GJ, Dias S, Lam G, et al. Arsenic trioxide induces dose- and time-dependent apoptosis of endothelium and may exert an antileukemic effect via inhibition of angiogenesis. Blood 2000;96:1525–30.
[49] Huynh TT, Sultan M, Vidovic D, et al. Retinoic acid and arsenic trioxide induce lasting differentiation and demethylation of target genes in APL cells. Sci Rep 2019;9:9414.
[50] Sanz MA, Fenaux P, Tallman MS, et al. Management of acute promyelocytic leukemia: updated recommendations from an expert panel of the European Leukemia Net. Blood 2019;133:1630–43.
[51] Yanada M, Matsushita T, Asou N, et al. Severe hemorrhagic complications during remission induction therapy for acute promyelocytic leukemia: incidence, risk factors, and influence on outcome. Eur J Haematol 2007;78:213–9.